Journal of Cardiovascular Magnetic Resonance (2007) **9,** 525–537

ISSN: 1097-6647 print / 1532-429X online
DOI: 10.1080/10976640601187604

informa
healthcare

Imaging Sequences for First Pass Perfusion—A Review

Peter Kellman, PhD and **Andrew E. Arai, MD**

Laboratory of Cardiac Energetics, National Heart, Lung and Blood Institute, National Institutes of Health, Department of Health and Human Services, Bethesda, Maryland, USA

ABSTRACT

Myocardial perfusion imaging sequences and analysis techniques continue to improve. We review the state-of-the-art in cardiovascular magnetic resonance first pass perfusion pulse sequences including the application of parallel imaging. There are a wide range of sequence designs and parameters to consider when optimizing an acquisition protocol. The interdependence of these parameters forces the user to make compromises. We describe the technical issues and provide insights into the various performance tradeoffs. We also review the basic design for T1-weighted first pass myocardial perfusion imaging and go on to discuss the tradeoffs associated with various schemes to provide multi-slice coverage. Artifact mechanisms are discussed and related to sequence design and parameters. The selection of quantitative versus qualitative analysis affects various performance requirements, such as spatial and temporal resolution and linearity of enhancement. Understanding the interaction between the pulse sequence parameters and resulting image quality is important for improving myocardial perfusion imaging.

INTRODUCTION

Myocardial perfusion imaging using cardiovascular magnetic resonance (CMR) has undergone steady improvement since it was first proposed over 20 years ago (1, 2). Yet there remain challenges for widespread clinical acceptance, and there is still considerable debate as to which technique is best. We review the state-of-the-art first pass perfusion pulse sequences including the application of parallel imaging for accelerated acquisition. Performance optimization is difficult due to the large number of parameters affecting image acquisition. Furthermore, the interdependence of these parameters forces the user to make compromises. As the field has not come to clear methodological consensus, we do not answer the debate on which is the best method. Rather, we describe the technical issues and provide insights into the various performance tradeoffs.

To maintain a focus on first pass perfusion methods, only certain topics could be included in this review. We start with the basic design for T1-weighted first pass myocardial perfusion imaging, and go on to discuss the tradeoffs associated with various schemes to provide multi-slice coverage. Artifact mechanisms are discussed and related to the sequence design and parameters. For simplicity, we consider only gadolinium based extracellular contrast agents, although there may be advantages to alternative contrast agents.

Both qualitative and quantitative analysis is considered in determining the various performance requirements, such as spatial resolution, temporal resolution, and T1-linearity. The topic of image analysis is another source of debate, and there remain questions on the value and accuracy of various performance indices. For issues beyond those dealt with in the current review, there is an abundance of literature on myocardial perfusion imaging, including original research on imaging methodology (3–17), comparisons between methods (18–22), review papers (23–27), and papers dealing with the subject of quantitative perfusion analysis (26, 28–33).

MYOCARDIAL PERFUSION IMAGING

Myocardial perfusion imaging is based on measuring the delivery of contrast agent to the myocardium during the first pass following a bolus injection. The signal intensity is enhanced

Keywords: Myocardial Perfusion, Cardiovascular MR, Ischemia, Parallel Imaging.
Supported by a grant from the National Heart, Lung, and Blood Institute, National Institutes of Health, Intramural Research Program
Correspondence to:
Peter Kellman
Laboratory of Cardiac Energetics
National Institutes of Health
National Heart, Lung and Blood Institute
10 Center Drive, MSC-1061
Building 10, Room B1D416
Bethesda, MD 20892-1061
tel: (301) 496-2513; fax (301) 402-2389
email: kellman@nih.gov

by the contrast agent, which shortens the T1 relaxation time and results in a brighter signal using a T1-weighted imaging sequence. Regions with lower regional blood flow will appear hypointense and may be detected given adequate image quality. Quantitative measurement of blood flow may be made through analysis of the dynamics of the myocardial signal intensity measurement as a function of time. Myocardial flow reserve may be estimated by comparing the flow measurements acquired at rest and at stress. Stress perfusion is most commonly studied using vasodilation such as adenosine or dipyridamole. Vasodilators increase the blood flow in normal vessels while stenotic vessels have a reduced vasodilator response.

Regions with prior myocardial infarction may appear hypointense despite normal blood flow, following revascularization, due to the low flow into scar tissue. Therefore, the interpretation of perfusion images usually also incorporates viability assessment by delayed enhancement imaging as described in the section on analysis.

Imaging requirements

Successful myocardial perfusion imaging requires optimizing sequence and parameters to meet often contradictory requirements. The basic requirements are:

1. **Temporal Resolution** Two distinct measures of temporal resolution are important for perfusion imaging. The time between two images of the same slice location affects the ability to sample the dynamic signal intensity changes during the first pass to allow modeling the kinetics of blood flow to the myocardium. Typically, images are acquired every 1–2 heartbeats to adequately sample myocardial blood flow. For quantitative perfusion, an accurate estimate of the arterial input function may require sampling the LV blood signal every heartbeat. Also of importance is the time per slice (T_{slice}) within the cardiac cycle, and the actual duration of imaging readout ($T_{imaging}$), which determines the sensitivity to cardiac motion, both indicated in Fig. 1a.
2. **Spatial Resolution** The spatial resolution must be adequate to distinguish sub-endocardial ischemia (<3 mm in-plane) and to assess transmural extent of defects.
3. **Spatial Coverage** It is desirable to have full coverage of the heart. A minimum of 3 slices is needed to cover at least 16 segments of the heart (34). A greater number of slices are desirable.
4. **Linearity** A linear or quantifiable relationship between signal intensity and contrast agent concentration is desirable in order to quantify perfusion.
5. **Image Quality** Image quality must be sufficient to provide contrast between normal and ischemic regions and must be free of artifacts.

A desire to quantify myocardial perfusion imposes additional requirements regarding accurate knowledge of the arterial input function, which represents the delivery of contrast to the heart and is commonly estimated from the blood signal. Therefore, quantitative myocardial perfusion imaging requires measuring both the blood and myocardial signals. The blood and myocardium have different contrast agent concentrations as well as T1, T2, and T2* relaxation parameters leading to significantly different imaging characteristics and signal intensities. The contrast between blood and myocardium is also affected by blood flow.

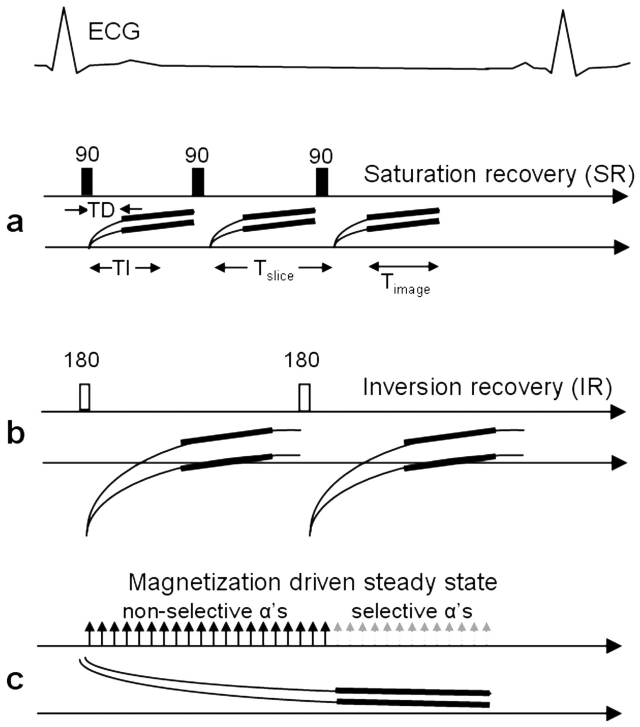

Figure 1. Magnetization preparation schemes for T1-weighted myocardial perfusion imaging: (a) saturation recovery (SR), (b) inversion recovery (IR), and (c) magnetization driven steady state.

T1-weighted imaging sequences

First-pass perfusion imaging typically acquires multiple slices of T1-weighted images that portray perfusion. Ideally, the signal intensity on such images should closely reflect the temporal change of the contrast agent concentration, which is inversely related to the achieved T1 ([Gd] $\sim$ 1/T1). A saturation recovery (SR) preparation (Fig. 1a) is the most commonly implemented method to achieve T1-weighting and may be used in conjunction with various methods for image readout.

In early work, inversion recovery (IR) approaches (Fig. 1b) were used (7–9, 17, 35, 36). IR approaches have the potential for increased dynamic range but are vulnerable to R-R variation or missed triggers which will cause signal intensity variation due to incomplete magnetization recovery. With IR preparation, the images are usually acquired at a time following inversion (TI) which nulls the pre-contrast blood to maximize the contrast and to avoid loss of contrast, which might result from magnitude detection. This results in a comparatively long imaging duration and commonly limits the imaging to a single slice per heartbeat.

In both SR and IR preparation schemes, there is generally a trigger delay (TD) between the RF preparation and the start of the image acquisition. In most cases, the signal intensity is determined by the delay to the center of k-space, which is commonly in the center of readout for linear phase encode ordering. This time is often referred to as the inversion time (TI) even in cases of SR preparations. While TD and TI are closely related, the literature contains reference to both often making direct comparisons difficult.

An alternative magnetization driven steady state preparation approach (Fig. 1c) was proposed (10) to achieve a higher degree of linearity than IR (i.e., signal intensity vs [Gd]). However, linearity was achieved at the expense of contrast-to-noise ratio (CNR) and had a lengthy preparation time limiting the acquisition to a single slice per heartbeat. In this scheme, the longitudinal magnetization was driven to steady state by a series of RF (alpha) pulses, followed by the readout. The preparation used non-selective RF pulses to reduce the effects of flow and motion. In the steady state limit, the signal intensity is linearly proportional to 1/T1 when using 90° readout pulses and was found to be quite linear using 45° readout, providing increased sensitivity (improved SNR) with only slight compromise in linearity (10).

Hybrid T1-preparation schemes

A number of hybrid preparation schemes can achieve T1-weighting with specific advantages and disadvantages. Arrhythmia insensitive approaches which combine SR preparation with IR have been proposed (Fig. 2a) (37). This scheme increases the length of preparation thereby reducing the number of slices that may be covered. By using a 90° SR preparation, which sets the longitudinal magnetization to zero, the 180° IR preparation which follows after a fixed short recovery period becomes insensitive to the RR interval. The dynamic range is somewhat compromised depending on the saturation recovery delay.

The magnetization driven steady state scheme may also be used with a 90° SR preparation (Fig. 2b) to reduce the time required to reach steady state. However, the linearity is still achieved at the expense of contrast-to-noise ratio (CNR) and slightly longer time per slice.

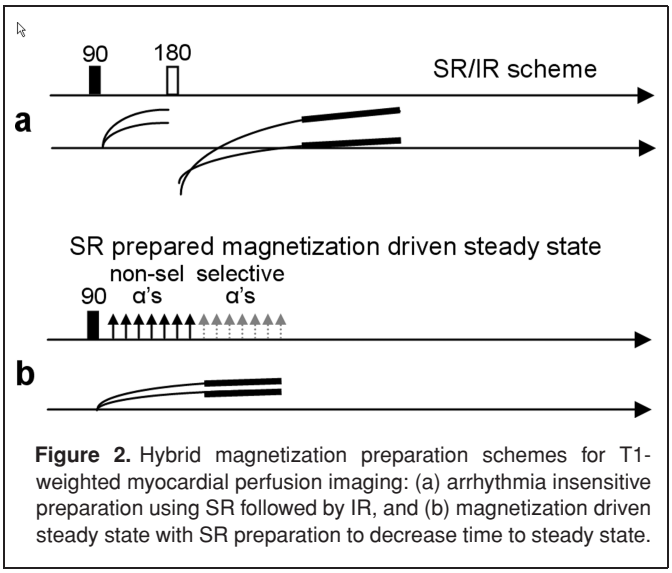

Figure 2. Hybrid magnetization preparation schemes for T1-weighted myocardial perfusion imaging: (a) arrhythmia insensitive preparation using SR followed by IR, and (b) magnetization driven steady state with SR preparation to decrease time to steady state.

Multi-slice approaches

There are several approaches to providing multi-slice coverage during first-pass imaging as shown in Fig. 3 for SR preparation. Other preparation schemes might be implemented as well if the time per slice permits. In each of these schemes, imaging is performed across the cardiac cycle; therefore, each slice will be acquired at a different phase of the cardiac cycle. Thus, the wall thickness and motion will vary slice-to-slice using these approaches. While it is possible to acquire fewer slices with less variation, for instance, only during diastole, this may reduce the overall spatial coverage, particularly if single RR temporal resolution is required. Furthermore, diastolic images have reduced wall thickness placing a higher demand on spatial resolution.

Using a single SR preparation per slice (Fig. 1a) provides reasonable coverage with uniform image quality. Approaches that acquire multiple slices per SR preparation offer increased efficiency. In one approach, multiple slices are readout sequentially following a single shared SR preparation (Fig.3b) (38, 39). In this scheme the TI varies from slice-to-slice and thus the T1-weighted contrast, CNR, and linearity all vary slice to slice. This scheme does reduce the time per slice slightly providing greater spatial coverage. A second approach which acquires multiple

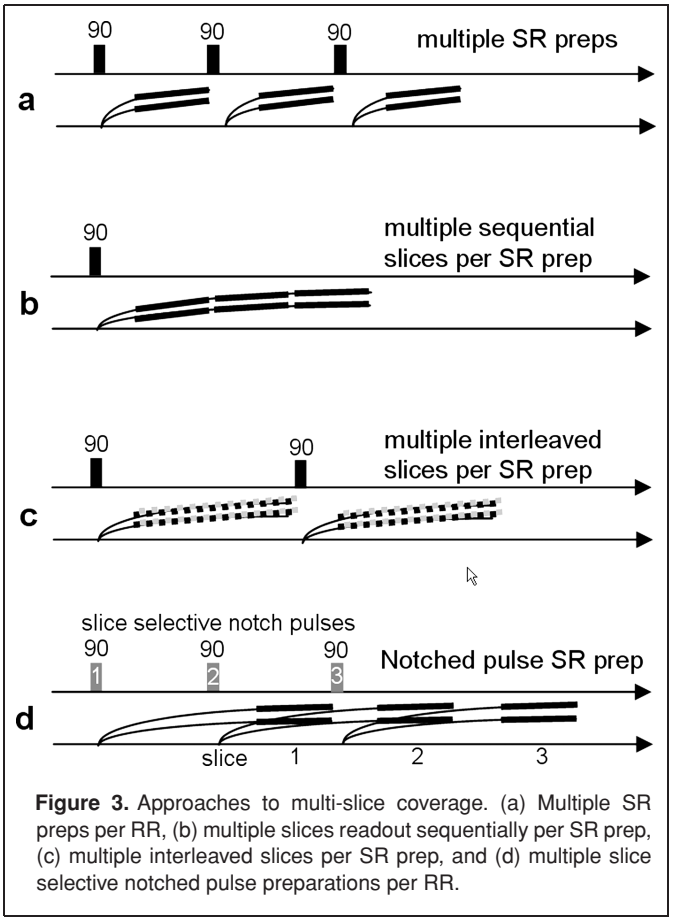

Figure 3. Approaches to multi-slice coverage. (a) Multiple SR preps per RR, (b) multiple slices readout sequentially per SR prep, (c) multiple interleaved slices per SR prep, and (d) multiple slice selective notched pulse preparations per RR.

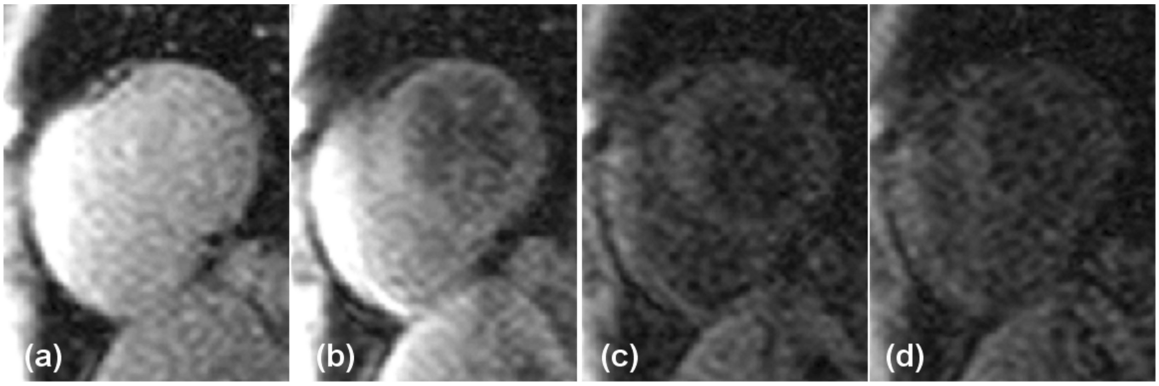

Figure 4. Saturation performance comparison of different SR prep pulses for GRE-EPI perfusion sequence with TI = 85 ms. (a) proton density reference without SR prep, (b) 90° SR prep pulse demonstrating B1 inhomogeneity and incomplete saturation, (c) sequel of 3 each 90° RECT pulses, (d) BIR4 adiabatic SR prep. All images are window-leveled the same. Incomplete saturation is evident using the 90° RECT (b).

slices per SR preparation acquires multiple interleaved slices (e.g., 2 slices) (Fig. 3c) (11). In this scheme, the TI remains constant. Although this approach increases the acquisition efficiency and thus spatial coverage, the actual imaging time per individual slice is increased thereby increasing the sensitivity to motion artifacts. A benefit of slice interleaving is the lengthening of the pulse repetition time (TR) between pulses of the same slice. An increased TR permits greater magnetization recovery and use of a higher readout flip angle for improved SNR.

A novel scheme for multi-slice coverage uses selective notch pulse preparations (15) where each notch selective SR preparation is used to prepare the 2nd slice following the saturation pulse (Fig. 3d). In this scheme, the selective notch pulse saturates the volume except for the next slice to be imaged. Thus, the saturation preparation for any given slice was played out prior to the previous slice readout. In this way, the preparation time (TI) may be made longer without requiring the overhead of a trigger delay. A longer TI may result in increased SNR although this comes at the cost of reduced linearity. A problem with this scheme is that the first slice may need to be discarded due to RR variations, eroding some of the efficiency gain. Furthermore, the selective notch pulse frequently results in non-uniform blood pool signal intensity due to heterogeneous through plane motion. Myocardial signal intensity is also sensitive to through plane motion, either cardiac or respiratory related.

Saturation recovery preparation

The 90° SR preparation is commonly used since an ideal 90° SR is insensitive to arrhythmia and/or missed ECG triggers. SR preparations using a lower flip angle (60°–70°) have been reported (3, 5) in cases of very short TD (10–15 ms) increasing sensitivity to RR variation. The 90° SR provides improved CNR given an adequate TI (3).

A few RF pulse designs have been proposed to achieve the ideal 90° SR preparation in the presence of B1-field inhomogeneity. The adiabatic BIR4 pulse provides improved insensitivity to both B1 and B0 (40, 41). The BIR4 has excellent performance as long as the adiabatic condition is achieved (i.e., adequate power). Alternatively, a pulse sequel design with several repeated 90° rectangular pulses with gradient crushers (42) improves the overall effectiveness of the saturation pulse in the event that the 90° rectangular pulse is not a true 90° due to B1-field inhomogeneity. In our experience both of these approaches are very effective and make a significant improvement over the simple 90° rectangular pulse (Fig. 4). The sensitivity to RR variation is illustrated in Fig. 5, which shows the effect of missed ECG triggers on the signal intensity for both 90° rectangular SR preparation and pulse sequel (3 pulses) with imperfect 90° pulses. The effect of missed ECG triggers is insignificant for the pulse sequel design.

The gradient crushers used in conjunction with the SR preparation RF pulse can lead to stimulated echo artifacts which degrade image quality. Stimulated echo artifacts due to these gradients may be mitigated by use of variable crushers.

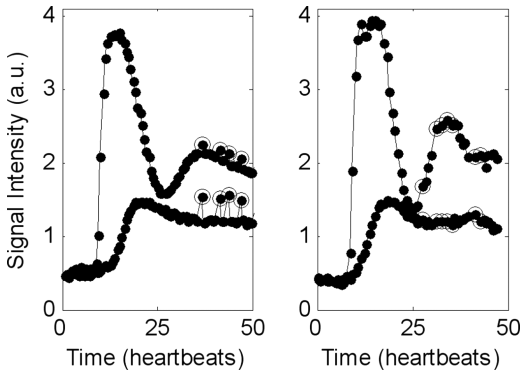

Figure 5. Time intensity curves for 2 cases with missed ECG triggers showing (a) sensitivity of signal intensity to missed triggers using 90 RECT SR prep with incomplete saturation (left) and (b) insensitivity to missed triggers using pulse sequel for SR prep (right). Incomplete saturation causes increased intensity following missed trigger (left). Samples following missed ECG trigger are marked with circles.

The saturation performance of the 90° SR preparation is particularly important for semi- and fully-quantitative perfusion measurements which rely on accurate baseline correction. Imperfect saturation biases the pre-contrast baseline by an amount that is not readily correctable.

Image readout & parallel imaging

Myocardial perfusion imaging sequences have been developed using IR or SR recovery in combination with either snapshot FLASH (7, 8), GRE-EPI (5), or balanced steady state free precession (SSFP, also known as FISP, FIESTA, or Balanced FFE) (13). There is no clear consensus regarding the sequence of choice for myocardial perfusion imaging, although there is considerable debate and several published comparisons (18–22).

There are also a number of approaches to parallel imaging (43–47) and other accelerated imaging methods (48–50) that may be applied to myocardial perfusion imaging. The application of parallel imaging is closely coupled with the image readout since the number of phase encodes may be substantially reduced, thus, altering the optimization of sequence parameters normally associated with the readout. The optimum choice of methods is a difficult question due to the large parameter space for each method and differing details of implementation between institutions and vendor platforms. It is not the objective of this paper to answer this debate. Rather, it is to review the current methods in light of advances, such as parallel imaging, and to highlight the pros and cons and performance issues.

Tradeoffs between spatial resolution and SNR, spatial and temporal resolution, and so on, are quite familiar in CMR. With the addition of the SR preparation, the number of variables and their interdependence grows. For example, a longer TI may increase the SNR but reduce the linearity of signal intensity vs contrast agent concentration (see below section). Some sequences have been optimized for linearity (10) while others have been optimized for CNR (3). In general, a longer TI will also reduce the spatial coverage. While one can optimize sequence parameters for SNR, coverage, and resolution, the interplay of sequence parameters and image artifacts is less understood. As described later, the presence of image artifacts in myocardial perfusion imaging is a large factor limiting clinical acceptance. The choice of readout and sequence parameters affects the point spread function (PSF) and other artifact mechanisms. The PSF is the term used to describe imperfect mapping between points on the object to the image, which may cause blurring or artifacts in the image.

In order to illustrate the influence of sequence parameters, an example is presented comparing SSFP, FLASH, and GRE-EPI readouts, all accelerated with SENSE parallel imaging at rate R = 2 (43, 44). The sequence parameters (Table 1) are based on values from current state-of-the-art implementations reported in the recent literature (21, 51) and are based on high performance gradients capable of 45 mT/m at 200 mT/m/ms slew rate. This example serves to illustrate the relative SNR and CNR, linearity, and the uniformity of k-space which affects the PSF.

Table 1. Myocardial perfusion sequence imaging parameters.

Method	SR-SSFP	SR-FLASH	SR-GRE-EPI
TE (ms)	1.1	1.3	1.1 (TE1)
TR (ms)	2.3	2.2	6.1
BW (Hz/pixel)	1400	780	1630
Echotrain length	1	1	4
Readout Flip Angle	50	12	25
Matrix	128 × 80	128 × 80	128 × 80
Parallel Imaging	R = 2	R = 2	R = 2
TD (ms) (to 1st line)	39	41	54
TI (ms) (to center)	85	85	85
$T_{imaging}$ (ms)	92	88	61
T_{slice} (ms) (total)	132	130	117
Slices per RR @ 60/90/120 bpm	7/5/3	7/5/3	8/5/4

In these examples, the matrix size = 128 × 80, and the TI = 85 ms. Both are held constant between sequences. All the sequences provide similar spatial coverage (slices per RR), with the GRE-EPI providing slightly greater coverage at the highest heart rates due to the increase acquisition efficiency of an EPI readout (T_{slice} = 117 ms vs 130 or 132 ms). The most significant difference given these parameters is the actual imaging duration within the cardiac cycle ($T_{imaging}$), which ranges from 61 ms for GRE-EPI to 92 ms for SSFP. The imaging duration may contribute to motion induced artifacts especially near the endocardium. Selection of the bandwidth (BW) is a tradeoff between the SNR and minimizing TR which affects $T_{imaging}$, T_{slice}, and number of slices per RR. It also affects the TE which in turn determines the $T2^*$ loss at peak contrast concentrations and the sensitivity to off-resonance due to B0-inhomogeneity and bolus susceptibility. TE is particularly important for a SSFP readout. While CNR is an important factor that depends on the $\sqrt{BW}$, the reduction of artifacts due to motion sensitivity (proportional to $T_{imaging}$) was judged to be of paramount importance. The TR period which consists of the RF pulse and actual readout decreased with increasing BW, reaching a point where the overhead of the RF pulse duration is a significant fraction. At this point, there is diminishing return in further BW increase. In this example (Table 1), the BWs were selected accordingly. Using a constant readout flip angle, the value of flip angle was selected for best uniformity of k-space response. Alternatively, a ramped or other variable readout flip angle might be considered.

The simulated responses of myocardial signal intensity are shown in Fig. 6 for varying contrast agent concentrations from 0 to 4 mmol/L, where the expected concentration in the myocardium is in the range 1–2 mmol/L for single dose (0.1 mmol/kg). Simulations used the method by Sekihara (52) with precontrast T1 = 850 ms and T2 = 50 ms in the myocardium, and 4.5 $(\text{sec mmol/L})^{-1}$ relaxivity of Gd based contrast agent. Note that the 40 actually acquired phase encodes are reconstructed to a full resolution of 80 lines by means of parallel imaging. Non-uniformity of the k-space response due to SR recovery and transient approach to the steady state of the readout leads to distortion of the PSF. Distorted PSF may cause edge artifacts or ghosting. The GRE-EPI has been reordered based on a modified center-out phase encode order (5)

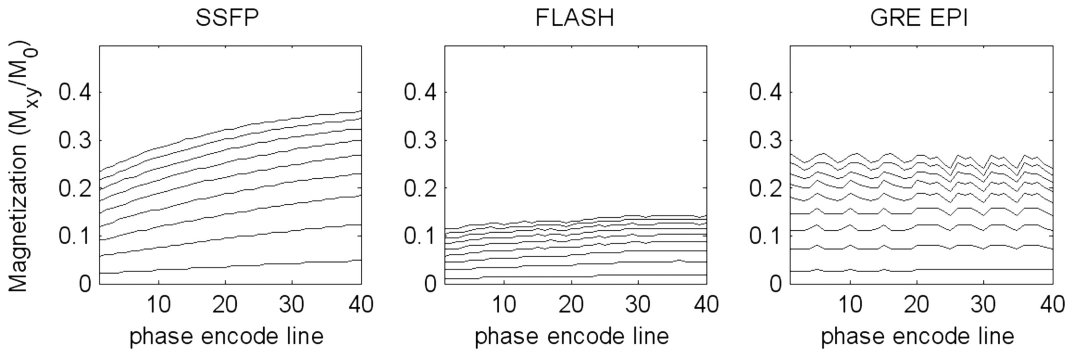

Figure 6. Simulated magnetization for SR myocardial perfusion imaging sequences with SSFP (left), FLASH (center), and GRE-EPI (right) readouts (parameters in Table 1) for contrast agent concentration ranging from 0 to 4 mmol/L (in 0.5 steps). Note that these plots represent magnetization signal and must be scaled by $\sqrt{}$(BW) to compare relative SNR. The actual number of acquired phase encodes = 40 is reconstructed to 80 using R = 2 parallel imaging.

chosen to acquire the central portion of k-space on the first echo (TE1) of the echotrain, thereby minimizing T2* losses and flow sensitivity. This results in a rapid periodic fluctuation in k-space which may lead to ghosting if the amplitude is too large.

The SSFP readout has the greatest signal (transverse magnetization), while the FLASH readout has the least signal. The SNR and CNR must also factor in the bandwidths (see following section).

The imaging parameters may be selected to meet different criteria. Note that the TI for each sequence might be varied to effect greater uniformity across k-space or variable readout flip angle might be considered. It may be noted that the SSFP sequence achieves higher SNR than GRE-EPI for instance, but requires a longer acquisition time. The SSFP sequence might be accelerated at R = 3 reducing $T_{imaging}$ from 92 ms to 61 ms (same as GRE-EPI) trading SNR for speed, making the SSFP and GRE-EPI readout methods practically equivalent in imaging duration and SNR. The SNR decrease between R = 3 and 2 is $\sqrt{}$(3/2) considering the SNR loss of $\sqrt{}$R.

IMAGING PERFORMANCE

Spatial resolution & coverage

The tradeoff between spatial resolution and coverage for SR with various readouts is described in Fig. 7, which plots the number of slices acquired per RR at heart rates of 60, 90, and 120 bpm for various matrix sizes and parallel imaging acceleration rates. Using a 360 × 270 mm^2 rectangular FOV, the spatial resolution is 2.8 × 3.4 mm^2 using a 128 × 80 matrix size, and 1.9 × 2.8 mm^2 using a 192 × 96 matrix size. These calculations assume TI = 100 ms for 128 × 80 at rate = 1 (no acceleration), TI = 85 ms for 128 × 80 at rate 2, TI = 150 ms for 192 × 96 at rate 1, and TI = 125 ms for 192 × 96 at rate 2. Using a 192 readout resolution extends the TR from 2.3 to 2.6 ms for SSFP, 2.2 to 2.3 for FLASH, and 6.1 to 6.6 for GRE-EPI. All sequence methods may achieve 3 slices per RR coverage at 192 × 96 matrix size at 120 bpm using parallel imaging at rate = 2. Of course, the higher spatial resolution will decrease the SNR proportional to the voxel size. In our experience, vasodilated stress heart rates are considerably higher than rest. Thus, pulse sequence parameters

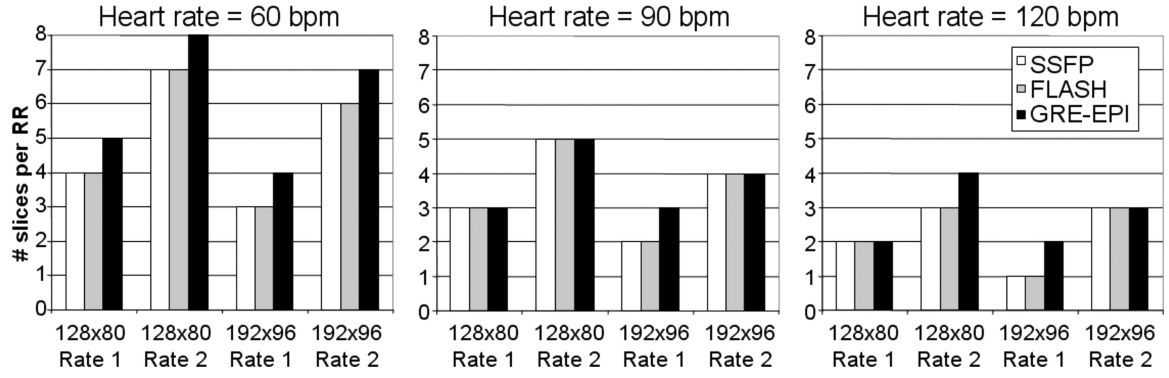

Figure 7. Spatial coverage and spatial resolution versus heart rate for SSFP, FLASH, and GRE-EPI sequences with and without parallel imaging. R = 2 denotes parallel imaging at acceleration rate 2, and R = 1 denotes no acceleration.

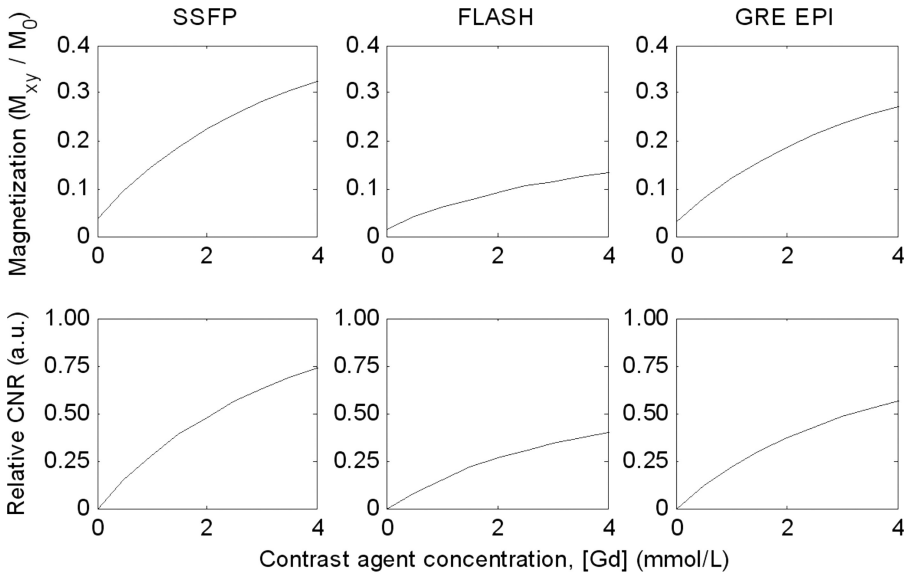

Figure 8. Relative CNR versus dose for SSFP, GRE-EPI, and FLASH readouts after baseline correction and scaling for bandwidth (sequence parameters per Table 1).

should be selected to achieve adequate spatial coverage at stress heart rates.

CNR & signal intensity linearity

The exponential recovery following saturation results in a non-linear relationship between signal intensity and contrast agent concentration. Ignoring the effect of readout on magnetization, the magnetization recovery following saturation is simply described by $M = [1- \exp(-TI/T_1)]$, with T_1 described by $(1/T_1) = (1/T_{1o}) + (\gamma\ [Gd])$, where $T_{1o} = 850$ ms is the pre-contrast T_1, and $\gamma = 4.5$ (sec mmol/L)$^{-1}$ is the relaxivity of Gd based contrast agent with concentration [Gd]. For $TI << T_1$, the magnetization is approximately proportional to [Gd] as seen by simple substitution, since $\exp(-TI/T_1) \approx (1 - TI/T_1)$. In the example (Table 1) with TI = 85 ms, there is already significant departure from linearity at [Gd] = 1.5 mmol/L where T1 $\approx$ 125 ms.

A more comprehensive simulation that accounts for magnetization effects of readout yields curves (Fig. 8) that demonstrate the non-linear relation versus contrast dose for the example sequence parameters listed in Table 1. The upper plots are the transverse magnetization without scaling for the bandwidth used in each sequence. The lower plots correspond to relative CNR after scaling for $\sqrt{BW}$ and correction of baseline intensity. The CNR for these plots is defined as signal difference between pre-contrast and post-contrast at a myocardial concentration of 2 mmol/L divided by the noise standard deviation. The CNR versus TI (Fig. 9) shows that small increases in CNR are possible with a large increase in non-linearity. Optimization for CNR without consideration of linearity and k-space uniformity will lead to selection of long TI (3).

The simulation for the parameters of Table 1 predicts that SSFP has approximately 40% higher CNR than GRE-EPI and 80% higher than FLASH, and GRE-EPI has approximately 40% higher CNR than FLASH. These predictions are fairly consistent with reported measurements using similar parameters (21) and with results that use FLASH with GRAPPA (45) parallel imaging (51) when factoring the effective acceleration used. For example (51), using R = 2 GRAPPA with 96 phase encode lines and 12 extra in-place reference lines results in an effective acceleration of R = 1.6.

The magnetization driven steady state approach (10) achieves a high degree of linearity even at 45° readout flip angle; however, the CNR penalty is estimated to be 50% or greater compared to SR-FLASH.

Artifacts

The presence of image artifacts in myocardial perfusion imaging is a large factor limiting clinical acceptance. In particular, artifacts that appear as a dark subendocardial rim (example

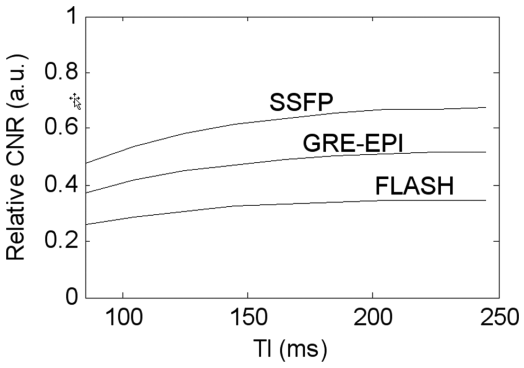

Figure 9. Relative CNR versus TI (between 0 and 2 mmol/L) for SSFP, GRE-EPI, and FLASH readouts after baseline correction and scaling for bandwidth (other parameters per Table 1).

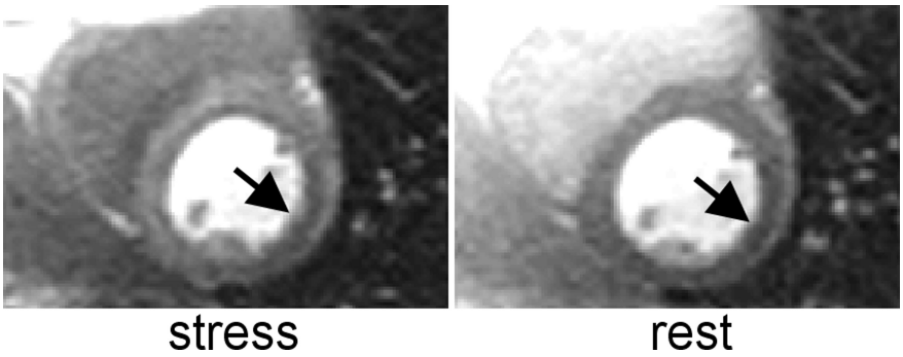

Figure 10. Dark rim artifact observed on both stress (left) and rest (right) studies using SR-SSFP for patient with negative cath (images courtesy of Jonathan Lyne, Royal Brompton Hospital, London).

Fig. 10) that may be confused with actual hypointense regions of reduced blood flow (53). Such artifacts can lead to false diagnoses and are of paramount concern. Strategies (54) have been articulated to help discriminate these artifacts (see next section). Understanding the artifact mechanisms may lead to sequence designs which minimize these deleterious effects.

Artifact mechanisms that may lead to dark sub-endocardial rim artifacts include cardiac motion (55) during the actual imaging period (T_{image}), Gibb's ringing (53) caused by truncation of k-space, non-uniformity of k-space weighting due to saturation recovery and readout, and partial volume cancellation between the myocardium and LV blood pool. Contribution of each of these artifact mechanisms is affected by the sequence and choice of parameters.

Minimizing cardiac motion artifacts may be accomplished either by using a small imaging duration ($T_{imaging}$) or by timing the acquisition to occur in periods with relatively low motion. Reducing the imaging duration may be accomplished by reducing the matrix size (low spatial resolution), using accelerated imaging such as parallel imaging, and using short TRs and/or EPI sequences. Diastole may provide a longer motion free window but comes at the cost of reduced left ventricular wall thickness thereby increasing the demand for better spatial resolution.

Gibb's ringing is generally mitigated to some extent by reconstruction with the use of raw filtering, also known as windowing or apodization. The ringing is suppressed at the expense of spatial resolution. In this case, it may be advantageous to acquire a larger matrix size and use a stronger raw filter (53). This will cost some spatial coverage but might be a worthwhile tradeoff. The extent of Gibb's ringing is determined by the step in intensity or contrast between the myocardium and blood. The SSFP sequence has a much higher blood-myocardium contrast, and therefore, will have commensurately larger ringing.

The non-uniformity across k-space (Fig. 6) leads to point spread function (PSF) distortion causing both blurring (loss of spatial resolution) and edge enhancement, which can cause dark rim artifacts. With the exception of the magnetization driven steady state (10) approach (Fig. 1[c]), myocardial perfusion imaging is not performed in a steady state condition, and the non-uniformity of the k-space response is determined by the tissue T1 values, TI, and readout flip angle. The dependence on T1 means that the PSF for the blood pool during peak bolus concentrations may be quite different than for the myocardium and may lead to rim artifacts at the sub-endocardial border between blood and myocardium. Ramp flip angle techniques might be considered to improve uniformity but are only effective for a single T1 value. In EPI sequences, which acquire at multiple echo times, the T2* loss at peak bolus concentration contributes to significant non-uniformity of k-space weighting for the blood pool signal. Non-uniform k-space weighting with the EPI phase encode order may lead to ghosting.

Partial volume effects may lead to dark rim artifacts when the blood and myocardium are out of phase. Spatial variation in phase may result from a number of effects including strong gradients in contrast agent concentration. These effects are related to the spatial resolution, therefore, it is desirable to have as many pixels transmurally as possible.

Other artifacts occur in addition to the dark rim artifact, although these may have less serious consequences. Using a SSFP readout, dark banding artifacts arise due to B0-field inhomogeneity caused by inadequate shim or susceptibility gradient associated with the bolus of contrast agent. Shim problems can be observed prior to contrast injection and mitigated by center frequency or shim re-adjustment. GRE-EPI readout is marred by ghosting due to off-resonance since there are phase shifts at each echo delay. This can be mitigated to a large extent by using an interleaved phase encode order with echo-time shifting (5). Chemical shift due to fat may cause ghosting; therefore, fat suppression pulses (56) are often used in conjunction with a GRE-EPI readout and can be implemented during the preparation time with little to no additional overhead. Stimulated echoes from the SR preparation may cause ghosting. Stimulated echoes may be eliminated by means of time varying gradient spoiling.

Aliasing artifacts or wrap due to accelerated imaging may lead to interference in the region of interest (Fig. 11). While these artifacts are generally recognized and therefore do not have

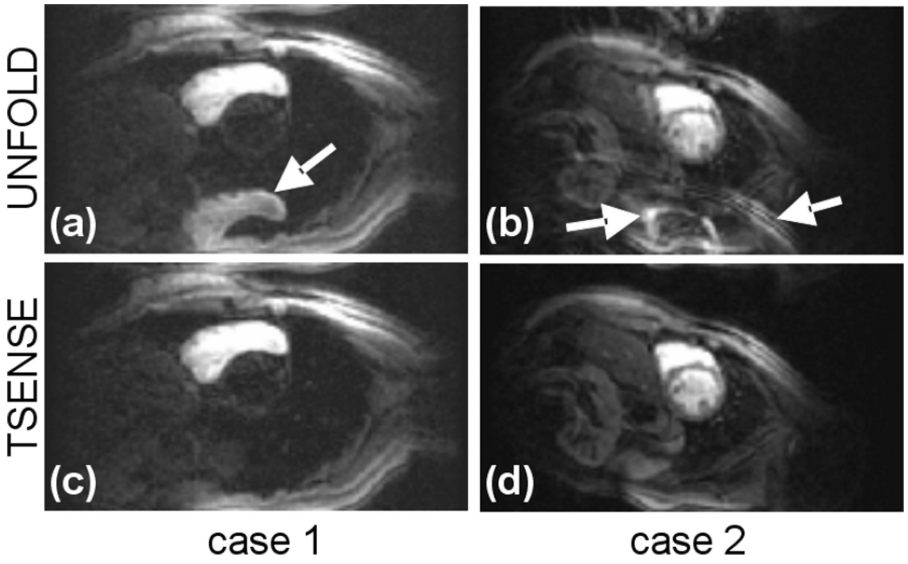

Figure 11. Examples images illustrating residual artifacts in UNFOLD reconstruction due to dynamic signal fluctuation. Case 1 illustrates UNFOLD artifact due to dynamic contrast enhancement of RV. Case 2 illustrates UNFOLD artifact due to breathing motion. In this example, these artifacts are suppressed with TSENSE parallel imaging.

the same consequence as the rim artifact, they may degrade the time intensity curves preventing accurate analysis. Since these artifacts may not appear until contrast is delivered, they can lead to non-diagnostic exams.

As illustrated in this section on artifacts, there are a wide range of factors that can result in artifacts. The worst artifacts result in subendocardial rims that can be misdiagnosed as perfusion defects. Factors that mitigate one mechanism generating rim artifacts may worsen another factor. For example, Gibbs ringing and partial volume errors can be improved by increasing image resolution, but higher spatial resolution may require longer readouts that exacerbate motion artifacts. Recognizing that some artifacts are worse during the time when concentration of gadolinium is highest in the ventricular cavities is important since this is a time when real perfusion defects should also be present.

ANALYSIS

Qualification

Qualitative assessment of myocardial perfusion deficit is rapid and has achieved diagnostic levels of sensitivity and specificity (54, 57–61) while quantitative analysis is currently more time consuming. A qualitative readout basically consists of examining the time course of images for evidence of hypointense regions.

Due to issues of noise and artifacts, additional interpretation strategies have been developed to minimize false positive diagnoses due to dark subendocardial rim artifacts. One strategy tested by the group at Duke University (54) combines stress and rest perfusion studies with delayed enhancement according to the following logic. Interpretation of coronary artery disease (CAD) begins with delayed enhancement. Positive delayed enhancement is a highly specific indicator of CAD. Negative delayed enhancements leads to examining the stress perfusion study. Negative delayed enhancement combined with negative stress perfusion results in a negative diagnosis for CAD. However, a positive stress perfusion deficit requires an analysis of rest perfusion. If the rest perfusion indicated that the hypointense region coincides with the stress perfusion hypointense region, then the result is qualified as a rim artifact, under the supposition that the rest study should have normal flow in regions without prior MI. Finally, an apparent stress perfusion deficit with normal rest perfusion would indicate CAD as illustrated in example of Fig. 12, which had no delayed enhancement. This strategy deals effectively with no prior recognized MI but does not address cases of ischemia in patients with prior MI. An example of stress and rest studies with a dark rim artifact is shown in Fig. 10, which was corroborated by a negative finding on a diagnostic catheterization (example provided by Jonathan Lyne and Peter Gatehouse, Royal Brompton Hospital).

The simple strategy outlined above may be further augmented by qualitative analysis of time intensity curves. This procedure required tracing endo- and epi-cardial contours to divide the myocardium into sectors. Each sector may be further subdivided transmurally into endo and epi layers. Tracing contours can be time consuming when there is respiratory motion. In this case, automatic registration methods may be applied (62, 63), although the performance of automatic registration is still improving.

Time intensity curves may be assessed qualitatively as well as quantitatively. For stress perfusion, the expected response for normal vessels with vasodilation show a peak (Fig. 13) in the myocardial signal intensity time course followed by a washout

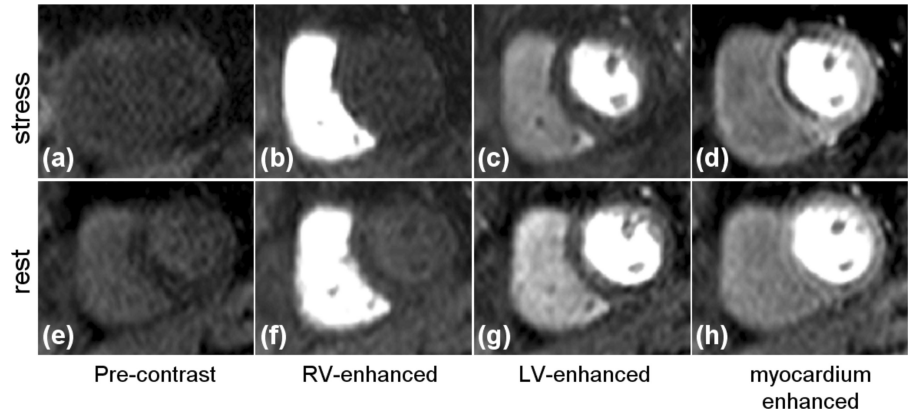

Figure 12. Example first-pass contrast-enhanced perfusion images for patient with stress perfusion deficit in antero-septal region shown for single slice of 3 acquired slices using GRE-EPI sequence using rate-2 TSENSE. The bottom row is at rest and top row is with stress: (a), (e) pre-contrast, (b), (f) RV enhanced, (c), (g) LV enhanced, and (d), (h) myocardium enhanced. Delayed enhancement images were negative for MI.

prior to the plateau. Absence of this overshoot indicates a lack of vasodilation and may be used to further augment the interpretation of findings based on visual image assessment.

Quantification

First-pass myocardial perfusion images may be used to characterize myocardial blood flow (MBF) using either fully or semi-quantitative methods. MBF (expressed in mL/min/g) and myocardial perfusion reserve (MPR) are defined as the ratio of hyperemic and resting blood flow. Both are clinically important indices for assessing myocardial ischemia, and are more objective than qualitative assessment. Fully quantitative myocardial blood flow (MBF) may be estimated using a Fermi model constrained deconvolution (29, 31, 32).

In order to quantify perfusion, it is necessary to have an accurate estimate of the arterial input function (AIF), which is normally measured from the LV blood pool signal. Due to non-linear effects of saturation recovery and T2* losses at high bolus concentration, the AIF estimated directly from the myocardial perfusion images becomes significantly distorted. For this reason, various solutions have been proposed. The dual-bolus first-pass perfusion method uses a high dose of contrast for myocardial analysis, preceded by a lower concentration bolus to maintain the linearity of the left ventricle (LV) signal intensity (29, 32). The dual sequence method (6, 12, 64), which acquires AIF reference images using a low TE and short saturation recovery delay, has been proposed to avoid distortion in the AIF. In the dual bolus method, a 1/20 dose mini-bolus has been found to provide an adequately linear response without noticeable distortion. The dual sequence method (Fig. 14) acquires low resolution blood pool images each heart beat requiring on the order of 60 ms, which slightly reduces the maximum spatial coverage. In order to maintain linearity at peak bolus concentration, it is necessary to have a TI on the order of 10 ms or less. This is accomplished using a center-out phase encode acquisition order with a short trigger delay to avoid edge enhancement due to highly non-uniform k-space response and a very low spatial resolution image. TE values on the order of 0.6 ms are used to minimize T2* distortion of the AIF (6, 64). T2* is estimated to be in the 6–12 ms range in the LV blood pool at peak concentrations for single dose (Fig. 15), corresponding to T2* losses of 5–10% using the dual sequence method with TE = 0.6 ms for the AIF measurement (65). The dual sequence method could be modified for greater spatial coverage by sampling of the myocardial perfusion signal every other heart beat while still maintaining single heartbeat temporal resolution for the AIF.

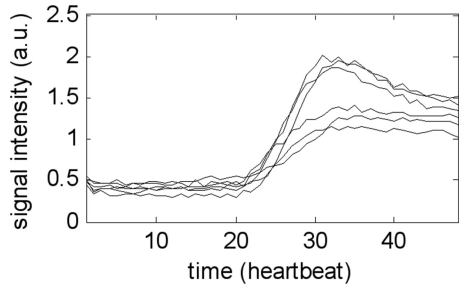

Figure 13. Time intensity curves for stress perfusion study (Fig. 12) using 6 endocardial sectors. Normal sectors show a vasodilated response, whereas the antero-septal region is hypo-intense.

The myocardial signal intensity does not have a linear relationship to [Gd] as desired due to T1-related effects. Although this has received less attention than the highly non-linear distortion of the blood pool signal, the effect of T1-nonlinearity on myocardial signal intensity may significantly affect perfusion quantification (66, 67). The myocardial perfusion signal non-linearity for SR sequences is largely determined by the TI as previously described and will affect the estimates of MBF even for relatively short TI (67). Look-up table (LUT) correction may be used to reduce the distortion providing more reliable flow estimates (66, 67). The LUT, which may be based on either

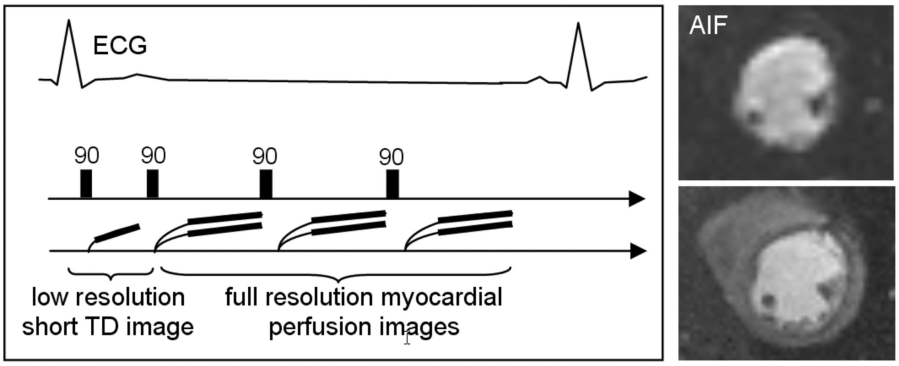

Figure 14. Dual sequence method for estimating arterial input function using a low resolution image with short TD for linear response of LV blood-pool signal at high Gd concentrations, and short TE to minimize T2* effects at peak bolus. Note that low spatial resolution AIF image (upper right) is adequate for sampling LV blood pool time intensity curve, but does not have adequate resolution to detect myocardial perfusion deficit (lower right image).

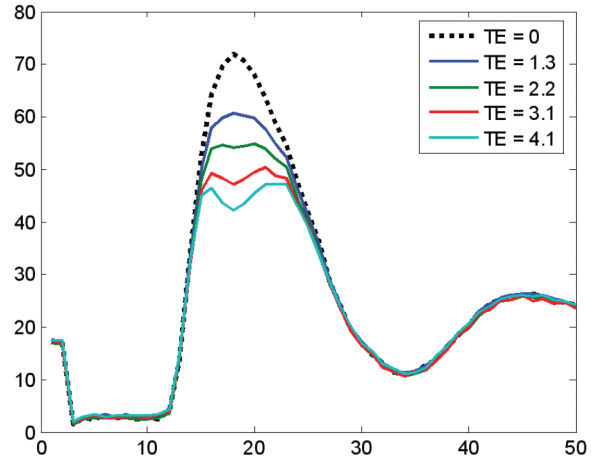

Figure 15. T2* effects observed in time intensity curves for LV blood pool ROI measured at different TE values using a multi-echo sequence. The TE = 0 curve (dotted line) is estimated based on a least squares fit to the multi-echo dataset. The initial 2 time frames are proton density reference images.

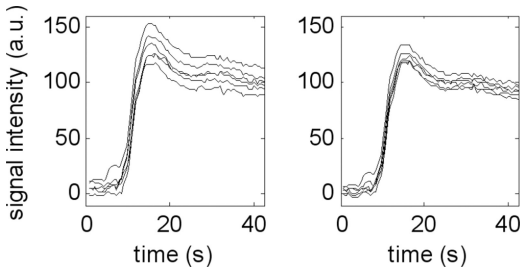

Figure 16. Correction of inhomogeneity due to surface coil intensity variation performed by scaling the raw myocardial time intensity curves (left) for each myocardial sector ROI by the value of the initial acquired proton density reference image for the same corresponding sector ROI (right).

theoretical or simulated curves, corrects the measured signal intensity for the non-linear relationship to Gd concentration.

Signal intensity variation due to surface coil B1-field inhomogeneity will affect quantitative assessment and must be factored into LUT correction of non-linear signal intensity response. Signal coil intensity correction may be implemented by normalization with proton density weighted images. Proton density weighted images may be acquired either in a separate pre-scan or as part of the myocardial perfusion imaging sequence at the initial frames just prior to the injection of contrast agent (using a low readout flip angle without SR preparation), ensuring image registration. Fig. 16 illustrates the time intensity curved before and after surface coil correction.

Typical acquisition of first-pass perfusion studies are 40-50 heartbeats in duration, which is too long for a single breath-hold in many patients. Registration of the images with endo and epi-cardial borders is, therefore, a critical step in generating high quality time intensity curves used in quantitative perfusion measurement (62, 63). Unless this step is reliably automated, this is the most time consuming aspect affecting the analysis.

A fully quantitative myocardial perfusion protocol generally includes both the stress and rest study in order to assess MPR and for qualitative interpretation of dark rim artifacts as previously described. The stress study, which is most critical, is performed first. There will be a residual concentration of contrast agent for the rest study, which is typically performed at least 10–15 minutes following the first bolus.

It is important to note that the measure of Gd contrast agent is detected indirectly through its effect on the 1H signal. Thus, water exchange between the vascular space, the interstitial space, and the intercellular space must be considered (68).

CONCLUSIONS

Myocardial perfusion imaging sequences and analysis techniques continue to improve. There are a wide range of sequence designs and parameters to consider in order to optimize an acquisition protocol. There is need for consensus on both sequence and

analysis in order to gain wider clinical acceptance and regulatory approval. There is also a need for common nomenclature. Dark rim artifacts may be minimized by careful design but remain a significant limitation of myocardial perfusion imaging and must be dealt with by objective assessment such as quantitative measurement or careful qualitative interpretation schemes.

REFERENCES

1. McNamara MT, Higgins CB, Ehman RL, Revel D, Sievers R, Brasch RC. Acute myocardial ischemia: magnetic resonance contrast enhancement with gadolinium-DTPA. Radiology 1984;153:157–63.
2. Atkinson DJ, Burstein D, Edelman RR. First-pass cardiac perfusion: evaluation with ultrafast MR imaging. Radiology 1990;174: 757–62.
3. Bertschinger KM, Nanz D, Buechi M, Luescher TF, Marincek B, von Schulthess GK, et al. Magnetic resonance myocardial first-pass perfusion imaging: parameter optimization for signal response and cardiac coverage. J Magn Reson Imaging 2001;14:556–62.
4. Debatin JF, McKinnon GC, von Schulthess GK. Technical note–approach to myocardial perfusion with echo planar imaging. Magma 1996;4:7–11.
5. Ding S, Wolff SD, Epstein FH. Improved coverage in dynamic contrast-enhanced cardiac MRI using interleaved gradient-echo EPI. Magn Reson Med 1998;39:514–9.
6. Gatehouse PD, Elkington AG, Ablitt NA, Yang GZ, Pennell DJ, Firmin DN. Accurate assessment of the arterial input function during high-dose myocardial perfusion cardiovascular magnetic resonance. J Magn Reson Imaging 2004;20:39–45.
7. Haase A. Snapshot FLASH MRI. Applications to T1, T2, and chemical-shift imaging. Magn Reson Med 1990;13:77–89.
8. Haase A, Matthaei D, Bartkowski R, Duhmke E, Leibfritz D. Inversion recovery snapshot FLASH MR imaging. J Comput Assist Tomogr 1989;13:1036–40.
9. Jivan A, Horsfield MA, Moody AR, Cherryman GR. Dynamic T1 measurement using snapshot-FLASH MRI. J Magn Reson 1997;127:65–72.
10. Judd RM, Reeder SB, Atalar E, McVeigh ER, Zerhouni EA. A magnetization-driven gradient echo pulse sequence for the study of myocardial perfusion. Magn Reson Med 1995;34:276–82.
11. Kellman P, Derbyshire JA, Agyeman KO, McVeigh ER, Arai AE. Extended coverage first-pass perfusion imaging using slice-interleaved TSENSE. Magn Reson Med 2004;51:200–204.
12. Kim D, Axel L. Multislice, dual-imaging sequence for increasing the dynamic range of the contrast-enhanced blood signal and CNR of myocardial enhancement at 3T. J Magn Reson Imaging 2006;23:81–6.
13. Schreiber WG, Schmitt M, Kalden P, Mohrs OK, Kreitner KF, Thelen M. Dynamic contrast-enhanced myocardial perfusion imaging using saturation-prepared TrueFISP. J Magn Reson Imaging 2002;16:641–52.
14. Schwitter J, Debatin JF, von Schulthess GK, McKinnon GC. Normal myocardial perfusion assessed with multishot echo-planar imaging. Magn Reson Med 1997;37:140–47.
15. Slavin GS, Wolff SD, Gupta SN, Foo TK. First-pass myocardial perfusion MR imaging with interleaved notched saturation: feasibility study. Radiology 2001;219:258–63.
16. Wendland MF, Saeed M, Masui T, Derugin N, Moseley ME, Higgins CB. Echo-planar MR imaging of normal and ischemic myocardium with gadodiamide injection. Radiology 1993;186:535–42.
17. Wendland MF, Saeed M, Yu KK, Roberts TP, Lauerma K, Derugin N, et al. Inversion recovery EPI of bolus transit in rat myocardium using intravascular and extravascular gadolinium-based MR contrast media: dose effects on peak signal enhancement. Magn Reson Med 1994;32:319–29.
18. Elkington AG, Gatehouse PD, Cannell TM, Moon JC, Prasad SK, Firmin DN, et al. Comparison of hybrid echo-planar imaging and FLASH myocardial perfusion cardiovascular MR imaging. Radiology 2005;235:237–43.
19. Fenchel M, Helber U, Simonetti OP, Stauder NI, Kramer U, Nguyen CN, et al. Multislice first-pass myocardial perfusion imaging: Comparison of saturation recovery (SR)-TrueFISP-two-dimensional (2D) and SR-TurboFLASH-2D pulse sequences. J Magn Reson Imaging 2004;19:555–63.
20. Wang Y, Moin K, Akinboboye O, Reichek N. Myocardial first pass perfusion: steady-state free precession versus spoiled gradient echo and segmented echo planar imaging. Magn Reson Med 2005;54:1123–9.
21. Weber S, Kronfeld A, Kunz RP, Fiebich M, Kreitner KF, Schreiber WG. Comparison of three accelerated Pulse Sequences for Quantitative Myocardial Perfusion Imaging using TSENSE. Proc Intl Soc Mag Reson Med 2006;14:206.
22. Hunold P, Maderwald S, Eggebrecht H, Vogt FM, Barkhausen J. Steady-state free precession sequences in myocardial first-pass perfusion MR imaging: comparison with TurboFLASH imaging. Eur Radiol 2004;14:409–16.
23. Barkhausen J, Hunold P, Jochims M, Debatin JF. Imaging of myocardial perfusion with magnetic resonance. J Magn Reson Imaging 2004;19:750–57.
24. Cuocolo A, Acampa W, Imbriaco M, De Luca N, Iovino GL, Salvatore M. The many ways to myocardial perfusion imaging. Q J Nucl Med Mol Imaging 2005;49:4–18.
25. Wilke N. MR measurement of myocardial perfusion. Magma 1998;6:147.
26. Wilke NM, Jerosch-Herold M, Zenovich A, Stillman AE. Magnetic resonance first-pass myocardial perfusion imaging: clinical validation and future applications. J Magn Reson Imaging 1999;10:676–85.
27. Canet EP, Janier MF, Revel D. Magnetic resonance perfusion imaging in ischemic heart disease. J Magn Reson Imaging 1999;10:423–33.
28. Axel L. Tissue mean transit time from dynamic computed tomography by a simple deconvolution technique. Invest Radiol 1983;18:94–9.
29. Christian TF, Rettmann DW, Aletras AH, Liao SL, Taylor JL, Balaban RS, et al. Absolute myocardial perfusion in canines measured by using dual-bolus first-pass MR imaging. Radiology 2004;232:677–84.
30. Jerosch-Herold M, Seethamraju RT, Swingen CM, Wilke NM, Stillman AE. Analysis of myocardial perfusion MRI. J Magn Reson Imaging 2004;19:758–70.
31. Jerosch-Herold M, Wilke N, Stillman AE. Magnetic resonance quantification of the myocardial perfusion reserve with a Fermi function model for constrained deconvolution. Med Phys 1998;25:73–84.
32. Hsu LY, Rhoads KL, Holly JE, Kellman P, Aletras AH, Arai AE. Quantitative myocardial perfusion analysis with a dual-bolus contrast-enhanced first-pass MRI technique in humans. J Magn Reson Imaging 2006;23:315–22.
33. Kostler H, Ritter C, Lipp M, Beer M, Hahn D, Sandstede J. Prebolus quantitative MR heart perfusion imaging. Magn Reson Med 2004;52:296–9.
34. Cerqueira MD, Weissman NJ, Dilsizian V, Jacobs AK, Kaul S, Laskey WK, et al. Standardized myocardial segmentation and nomenclature for tomographic imaging of the heart: a statement for healthcare professionals from the Cardiac Imaging Committee of the Council on Clinical Cardiology of the American Heart Association. Circulation 2002;105:539–42.
35. Fritz-Hansen T, Rostrup E, Ring PB, Larsson HB. Quantification of gadolinium-DTPA concentrations for different inversion times using an IR-turbo flash pulse sequence: a study on optimizing multislice perfusion imaging. Magn Reson Imaging 1998;16:893–9.

36. Wilke N, Simm C, Zhang J, Ellermann J, Ya X, Merkle H, et al. Contrast-enhanced first pass myocardial perfusion imaging: correlation between myocardial blood flow in dogs at rest and during hyperemia. Magn Reson Med 1993;29:485–97.

37. Tsekos NV, Zhang Y, Merkle H, Wilke N, Jerosch-Herold M, Stillman A, Ugurbil K. Fast anatomical imaging of the heart and assessment of myocardial perfusion with arrhythmia insensitive magnetization preparation. Magn Reson Med 1995;34:530–36.

38. Nagel E, Klein C, Paetsch I, Hettwer S, Schnackenburg B, Wegscheider K, et al. Magnetic resonance perfusion measurements for the noninvasive detection of coronary artery disease. Circulation 2003;108:432–7.

39. Fischer SE, Lorenz CH. [Determining heart muscle perfusion by magnetic resonance tomography progressing to clinical application]. Radiologe 1997;37:366–71.

40. Kim D, Cernicanu A, Axel L. B(0) and B(1)-insensitive uniform T(1)-weighting for quantitative, first-pass myocardial perfusion magnetic resonance imaging. Magn Reson Med 2005;54:1423–9.

41. Staewen RS, Johnson AJ, Ross BD, Parrish T, Merkle H, Garwood M. 3-D FLASH imaging using a single surface coil and a new adiabatic pulse, BIR-4. Invest Radiol 1990;25:559–67.

42. Oesingmann N, Zhang,Q. ,Simonetti, O. Improved Saturation RF Pulse Design for Myocardial First Pass Perfusion at 3T. Journal of Cardiovascular Magnetic Resonance 2004;6:373–4.

43. Pruessmann KP, Weiger M, Scheidegger MB, Boesiger P. SENSE: sensitivity encoding for fast MRI. Magn Reson Med 1999;42:952–62.

44. Kellman P, Epstein FH, McVeigh ER. Adaptive sensitivity encoding incorporating temporal filtering (TSENSE). Magn Reson Med 2001;45:846–52.

45. Griswold MA, Jakob PM, Heidemann RM, Nittka M, Jellus V, Wang J, et al. Generalized autocalibrating partially parallel acquisitions (GRAPPA). Magn Reson Med 2002;47:1202–10.

46. Kostler H, Sandstede JJ, Lipke C, Landschutz W, Beer M, Hahn D. Auto-SENSE perfusion imaging of the whole human heart. J Magn Reson Imaging 2003;18:702–8.

47. Tsao J, Boesiger P, Pruessmann KP. k-t BLAST and k-t SENSE: dynamic MRI with high frame rate exploiting spatiotemporal correlations. Magn Reson Med 2003;50:1031–42.

48. Epstein FH, Kellman P, McVeigh ER. First-pass Cardiac MRI using UNFOLD. Proc of RSNA Scientific Assembly and Annual Meeting. 2000; Chicago; 291.

49. Madore B, Glover GH, Pelc NJ. Unaliasing by fourier-encoding the overlaps using the temporal dimension (UNFOLD), applied to cardiac imaging and fMRI. Magn Reson Med 1999;42:813–28.

50. Di Bella EV, Wu YJ, Alexander AL, Parker DL, Green D, McGann CJ. Comparison of temporal filtering methods for dynamic contrast MRI myocardial perfusion studies. Magn Reson Med 2003;49:895–902.

51. Lyne JC, Assomull, R, Smith, GC, Gatehouse PD, Firmin DN, Pennell DJ. Comparison of EPI, TrueFISP, and FLASH Sequences with Parallel Acquisition for Myocardial Perfusion Imaging. Journal of Cardiovascular Magnetic Resonance 2006;8:113–4.

52. Sekihara K. Steady-state magnetizations in rapid NMR imaging using small flip angles and short repetition intervals. IEEE Trans on Med Imag 1987;6:157–64.

53. Di Bella EV, Parker DL, Sinusas AJ. On the dark rim artifact in dynamic contrast-enhanced MRI myocardial perfusion studies. Magn Reson Med 2005;54:1295–9.

54. Klem I, Heitner JF, Shah DJ, Sketch MH, Jr., Behar V, Weinsaft J, Cawley P, Parker M, Elliott M, Judd RM, Kim RJ. Improved detection of coronary artery disease by stress perfusion cardiovascular magnetic resonance with the use of delayed enhancement infarction imaging. J Am Coll Cardiol 2006;47:1630–8.

55. Storey P, Chen Q, Li W, Edelman RR, Prasad PV. Band artifacts due to bulk motion. Magn Reson Med 2002;48:1028–36.

56. Ingkanisorn WP, Rhoads KL, Syed, MA, Dyke, CK, Kellman P, Aletras AH, et al. Fat-Suppression Improves Image Quality and Diagnostic Accuracy of EPI First Pass Perfusion. Proc of Intl Soc Mag Res Med. 2004; Kyoto, Japan; 312.

57. Ingkanisorn WP, Kwong RY, Bohme NS, Geller NL, Rhoads KL, Dyke CK, et al. Prognosis of negative adenosine stress magnetic resonance in patients presenting to an emergency department with chest pain. J Am Coll Cardiol 2006;47:1427–32.

58. Ishida N, Sakuma H, Motoyasu M, Okinaka T, Isaka N, Nakano T, et al. Noninfarcted myocardium: correlation between dynamic first-pass contrast-enhanced myocardial MR imaging and quantitative coronary angiography. Radiology 2003;229:209–16.

59. Paetsch I, Foll D, Langreck H, Herkommer B, Klein C, Schalla S, et al. Myocardial perfusion imaging using OMNISCAN: a dose finding study for visual assessment of stress-induced regional perfusion abnormalities. J Cardiovasc Magn Reson 2004;6:803–9.

60. Takase B, Nagata M, Kihara T, Kameyawa A, Noya K, Matsui T, et al. Whole-heart dipyridamole stress first-pass myocardial perfusion MRI for the detection of coronary artery disease. Jpn Heart J 2004;45:475–86.

61. Wolff SD, Schwitter J, Coulden R, Friedrich MG, Bluemke DA, Biederman RW, et al. Myocardial first-pass perfusion magnetic resonance imaging: a multicenter dose-ranging study. Circulation 2004;110:732–7.

62. Dornier C, Ivancevic MK, Thevenaz P, Vallee JP. Improvement in the quantification of myocardial perfusion using an automatic spline-based registration algorithm. J Magn Reson Imaging 2003;18:160–8.

63. Gupta SN, Solaiyappan M, Beache GM, Arai AE, Foo TK. Fast method for correcting image misregistration due to organ motion in time-series MRI data. Magn Reson Med 2003;49:506–14.

64. Elkington AG, He T, Gatehouse PD, Prasad SK, Firmin DN, Pennell DJ. Optimization of the arterial input function for myocardial perfusion cardiovascular magnetic resonance. J Magn Reson Imaging 2005;21:354–9.

65. Kellman P, Aletras AH, Hsu L, McVeigh ER, Arai AE. T2* Measurement During First-Pass Contrast-Enhanced Cardiac Perfusion Imaging. Magn Reson Med 2006;56:1132–4.

66. Cernicanu A, Axel L. Theory-based signal calibration with single-point T1 measurements for first-pass quantitative perfusion MRI studies. Acad Radiol 2006;13:686–93.

67. Hsu LY, Kellman P, Arai AE. Correction for T1-Nonlinearity in Myocardial Signal Intensity Improves First-Pass Perfusion Quantification. Tenth Annual Scientific Sessions of SCMR. 2007; Rome, Italy.

68. Donahue KM, Burstein D, Manning WJ, Gray ML. Studies of Gd-DTPA relaxivity and proton exchange rates in tissue. Magn Reson Med 1994;32:66–76.